Journal of Colloid and Interface Science 695 (2025) 137751

Contents lists available at ScienceDirect

Journal of Colloid And Interface Science

journal homepage: www.elsevier.com/locate/jcis

Brain-targeted polymersomes mediating RNAi of STAT3 sensitize glioblastoma to temozolomide and immunotherapy

Mingyu Xia [a], Songsong Zhao [a], Zhiwei Sun [a], Yan Shi [a], Wenhai Lin [a], Zhiyuan Zhong [a,b,*], Fenghua Meng [a,*]

[a] Biomedical Polymers Laboratory, College of Chemistry, Chemical Engineering and Materials Science, and State Key Laboratory of Radiation Medicine and Protection, Soochow University, Suzhou 215123, PR China
[b] College of Pharmaceutical Sciences, Soochow University, Suzhou 215123, PR China

GRAPHICAL ABSTRACT

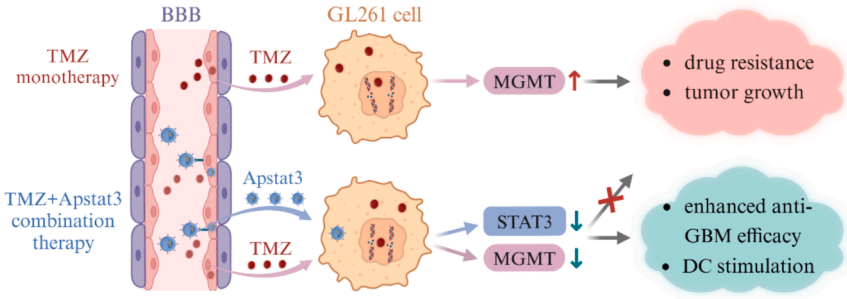

ARTICLE INFO

Keywords:
Glioblastoma
Drug resistance
Temozolomide
Targeted delivery
STAT3
Sensitization

ABSTRACT

Glioblastoma (GBM) is among the most aggressive brain tumors, presenting significant therapeutic challenges due to intrinsic and acquired resistance to treatment, alongside a highly immunosuppressive tumor microenvironment (TME). While temozolomide (TMZ) is the standard chemotherapeutic agent with the ability to penetrate the blood–brain barrier (BBB), its clinical efficacy is often limited. Here, we report a strategy employing Apolipoprotein E (ApoE) peptide-functionalized polymersomes loaded with small interfering RNA (siRNA) targeting signal transducer and activator of transcription 3 (Apstat3) to amplify the anti-GBM effects of TMZ and immunotherapy. Apstat3 demonstrated small, uniform particle sizes, stability in siRNA encapsulation, and effective downregulation of STAT3 and O^6-methylguanine-DNA methyltransferase (MGMT) in GL261 cells, sensitizing these tumor cells to TMZ. The combinatorial approach not only significantly inhibited GBM cell proliferation, migration and invasion but also improved dendritic cells (DCs) maturation under TME-mimicking environment. In orthotopic GL261 mouse models, intravenous injection of Apstat3 co-administered with oral TMZ resulted in a twofold increase in median survival and reshaped the TME. Notably, combined treatment with anti-CTLA4 therapy tripled median survival to 64 days, achieving complete remission observed in 20% of the mice. This siSTAT3 delivery strategy holds promise for enhancing GBM treatment outcomes.

* Corresponding authors at: Biomedical Polymers Laboratory, College of Chemistry, Chemical Engineering and Materials Science, and State Key Laboratory of Radiation Medicine and Protection, Soochow University, Suzhou 215123, PR China (Zhiyuan Zhong).
E-mail addresses: zyzhong@suda.edu.cn (Z. Zhong), fhmeng@suda.edu.cn (F. Meng).

https://doi.org/10.1016/j.jcis.2025.137751
Received 25 February 2025; Received in revised form 23 April 2025; Accepted 29 April 2025
Available online 1 May 2025

1. Introduction

GBM is one of the most aggressive and malignant brain tumors, posing formidable challenges for effective drug delivery due to the restrictive nature of the BBB [1]. TMZ is a first-line therapeutic agent known for its ability to cross the BBB. Traditional TMZ treatment regimens include monotherapy, combination with radiotherapy, and combination therapy with other drugs. However, clinical outcomes are often unsatisfactory, marked by disappointingly low response rates [2]. Compounding this issue, many patients develop inherent or acquired resistance during treatment, progressively diminishing their responsiveness to TMZ [3]. A critical mechanism driving this resistance is the upregulation of MGMT, a DNA repair enzyme that directly undermines TMZ's therapeutic efficacy [4]. Various strategies have been explored to sensitize GBM to TMZ [5–7], including clinical trials utilizing combination therapies such as lomustine with TMZ (NCT01149109) [8], and radiotherapy combined with TMZ and ralimetinib (NCT02364206) [9]. However, the overall efficacy of these therapies is hindered due to inefficient drug penetration across the BBB, inadequate accumulation within GBM cells, and a highly immunosuppressive TME.

Moreover, the STAT3 pathway plays a crucial role in mediating tumor invasion and immune evasion [10]. Aberrant activation of STAT3 is frequently observed in GBM cells and within the TME [11]. Targeting STAT3 represents a promising strategy to downregulate elevated MGMT levels, potentially overcoming drug resistance and enhancing antitumor efficacy [12]. Furthermore, STAT3 inhibition in immune cells, particularly dendritic cells (DCs), has been shown to significantly improve DC maturation and function [13]. Although small-molecule STAT3 inhibitors have shown some therapeutic potential, their clinical utility is often limited by rapid clearance and off-target effects [14]. RNA interference (RNAi) technology using small interfering RNA (siRNA) offers a compelling alternative by silencing specific genes. However, effective in vivo delivery of siRNA drugs remains a critical challenge [15]. Amphiphilic copolymer-based polymersomes have attracted considerable interest as nanocarriers for drug delivery [16], due to their structural stability, capacity to encapsulate diverse payloads including siRNA, and the ease of functionalization with targeting ligands [17,18].

In this study, we report an approach employing brain-targeted polymersomes to mediate RNAi of STAT3, thereby sensitizing GBM to TMZ while reshaping GBM immunosuppressive TME. We formulated ApoE peptide-functionalized polymersomes encapsulating siSTAT3 (Apstat3) from siSTAT3 and biodegradable dithiolane-containing copolymers, poly(ethylene glycol)-*b*-poly(trimethylene carbonate-*co*-dithiolane trimethylene carbonate)-spermine (PEG-P(TMC-DTC)-Spe) and ApoE peptide-functionalized ApoE-PEG-P(TMC-DTC). Apstat3 loads siSTAT3 through electrostatic interactions between siRNA and the polymersome inner shell. The ApoE peptides bind to low-density lipoprotein receptors (LDLRs), which are highly expressed in the BBB and GBM cells [19–21], facilitating BBB penetration and receptor-mediated endocytosis by tumor cells, thus achieving GBM-targeted delivery [22,23]. After endocytosis, Apstat3 undergoes reduction-triggered release in the cytosol, effectively silencing aberrantly expressed STAT3 in GBM tumors. This leads to the downregulation of MGMT and B-cell lymphoma-2 (Bcl-2), significantly enhancing the sensitivity of GBM cells to TMZ treatment and ameliorating drug resistance while promoting DC maturation (Scheme 1). Our in vivo experiments demonstrate that combining Apstat3 with TMZ greatly inhibits the progression of orthotopic GL261 tumors, and further addition of anti-CTLA4 therapy results in significant survival extension.

2. Materials and methods

2.1. Materials

Mouse STAT3 siRNA (siSTAT3, SS: 5′-CAGGGUGUCAGAUCACAGGGCUAA-chol-3′; AS: 5′-UUAGCCCAUGUGAUCUGACACCCUGAA-3′, Genepharma), cy5-labeled STAT3 siRNA (cy5-siSTAT3, Genepharma) and ApoE peptide (LRKLRKRLLLRKLRKRLLC, GL Biochem) were custom-synthesized with purities over 95%. Primers targeting murine STAT3 (Forward: 5′-TGTCAGATCACATGGGCTAAAT-3′; Reverse: 5′-GGTCGATGATATTGTCTAGCCA-3′), targeting murine Bcl-2 (Forward: 5′- GATGACTTCTCTCGTCGCTAC-3′; Reverse: 5′- GAACTCAAAGAAGGCCACAATC-3′), targeting murine MGMT (Forward: 5′- CAATTACATCATCCTCCCACCTTCAG-3′; Reverse: 5′- GCTCGTTCCTCCAATCGTATGC-3′) were custom-synthesized (≥95%) by Sangon Biotech. Temozolomide (TMZ, ≥98%, aladdin), L-glutathione (GSH, Ameresco), β-mercaptoethanol (Thermo), CCK-8 (meilune), RNase A (BioFroxx), (4,6-diamino-2-phenylindole (DAPI, Beyotime), CM-DIL (Yeasen) and transwell (Corning) were used directly. PEG-P(TMC-DTC)-Spe (M_n = 5.0-(14.9–2.0)-0.2 kg/mol) [24] and ApoE-PEG-P (TMC-DTC) (M_n = 7.5-(15.2–1.9) kg/mol) [25] were synthesized according to previous reports. DMEM/F-12 medium (Gibco), DMEM medium (Gibco), RPMI-1640 medium (Gibco), fetal bovine serum (FBS, Gibco), penicillin-ptreptomycin (Biosharp), accutase (BioLegend), matrigel (356231, Corning), lysotracker green DND-26 (Yeasen), RNA-easy Isolation Reagent (Vazyme), D-luciferin potassium salt (Meilunbio), Evans blue (Beyotime), and transforming growth factor-β (TGF-β, TargetMol) were used without further treatment.

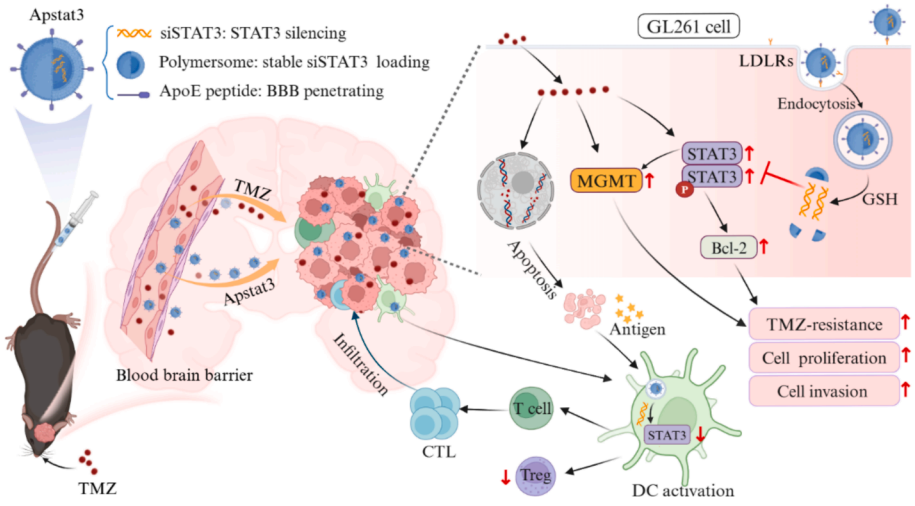

Scheme 1. Schematic illustration of the composition of ApoE peptide-functionalized siSTAT3 loaded polymersomes (Apstat3) and the combination with TMZ in treating mice bearing orthotopic glioblastoma. The figure was created using BioRender.

ELISA kits (Invitrogen) of mouse tumor necrosis factor-α (TNF-α) and interleukin-6 (IL-6), Pierce™ BCA Protein Assay Kit (Thermo Scientific), PAGE Gel Preparation Kit (Epizyme Biotech), enhanced efficient chemiluminescence kit (ECL, Absin) were used according to manufacturer's protocol. TGF beta 1 Protein (TMPY-00608) were purchased from TargetMol. Precision count beads and antibodies including APC-Cy7-Zombie NIR™ Fixable Viability Kit, anti-CD16/32-TruStain FcX™, FITC-anti-CD11c (N418), PE-anti-CD86 (PO3.1), APC-anti-CD80 (16-10A1), PE-anti-F4/80 (BM8), PE-anti-CD4 (GK1.5), PE/Cy7-anti-CD8a (53–6.7), and Alexa Fluor 647-anti-foxp3 (150D) were purchased from Biolegend. Other antibodies like anti-stat3 (124H6) (9139, CST), anti-phospho stat3 (Tyr705) (ab267373, Abcam), anti-MGMT (67476, Proteintech), anti-Bcl-2 (4223, CST), HRP labelled goat anti-rabbit secondary antibody (GB23303, Servicebio), and Alexa Fluor® 647 or Alexa Fluor® 488 labelled goat anti-rabbit IgG H&L secondary antibody (Invitrogen) were used according to supplier's protocol.

2.2. Cells and animals

Murine GL261 cells were provided by Prof. Jian Chen from Chinese Institute for Brain Research. Mouse microglial cells (BV2) and mouse brain microvascular endothelial cells (bEnd.3) were all purchased from the Shanghai Cell Bank of the Chinese Academy of Sciences. GL261 and BV2 cells were cultured in DMEM medium containing 10% fetal bovine serum (FBS) and 1% penicillin–streptomycin. bEnd.3 cells were cultured in a special medium from Procell (Pu Nuo Sai). When cell confluence reached 80%, cells were digested with 0.25% (w/v) trypsin containing 0.03% (w/v) ethylenediaminetetraacetic acid (EDTA) before use. Bone marrow-derived dendritic cells (BMDCs) were obtained from the femurs and tibias of 6–7-week-old female C57BL/6J mice as described [26].

All animal experiments were approved the Animal Care and Use Committee of Soochow University (P. R. China) and all protocols for the animal studies conformed to the Guide for the Care and Use of Laboratory Animals (202307A0300, 202503A0568).

2.3. Characterizations

The size, size distribution and zeta potential of polymersomes were measured using a Zetasizer Nano-ZS (Malvern Instruments) equipped with dynamic light scattering (DLS, with a 633 nm He-Ne laser using back-scattering detection) and electrophoresis capillary. The siSTAT3 loading of the polymersomes were determined by NanoDrop spectrophotometer (Thermo). A gel imaging system (Analytikjena, Germany) was used for agarose gel electrophoresis imaging and western blot (WB) imaging. An epithelial voltmeter (Millicell-ERS, Millipore) was used for detecting the trans-endothelial electrical resistance (TEER) of BBB monolayers. A microplate reader (Thermo Scientific Varioskan LUX) was used for CCK-8 assays and ELISA assays. Flow cytometry (FC) measurements were conducted on a flow cytometer (BD FACS Calibur) to study the uptake of polymersomes and stimulation of immune cells. A confocal laser scanning microscope (CLSM, TCS SP5, Leica) was used to study the endocytosis and endosomal escape of polymersomes. The mRNA expression in tumor cells was determined using a quantitative real-time polymerase chain reaction (qRT-PCR, CFX Connect™, Bio-rad). In vivo and ex vivo imaging were performed using a near-infrared fluorescence imaging system (IVIS Lumina II, Perkin Elmer).

2.4. Preparation and characterization of Apstat3

PEG-P(TMC-DTC)-Spe (M_n = 5.0-(14.9–2.0)-0.2 kg/mol) [24] and ApoE-PEG-P(TMC-DTC) (M_n = 7.5-(15.2–1.9) kg/mol) [25] were synthesized according to our previous reports, and dissolved separately in DMF (final polymer concentration of 40 mg/mL) before mixing at a mass ratio of 20/80. Typically, for preparing Apstat3 with ApoE peptide 20% and siRNA loading content of 10 wt.%, 10 μL polymer mixture was added into 390 μL phosphate buffer (PB, 2.0 mM, pH 6.0) containing 40 μg of siSTAT3 under mild stirring. Following dialysis for 6 h (MWCO 1000 kDa) to remove organic solvent and unloaded siRNA, Apstat3 was obtained and ready for further studies. The non-targeted control, Pstat3, was prepared similarly except from PEG-P(TMC-DTC)-Spe only. Cy5-labeled Apstat3 was prepared from ApoE-PEG-P(TMC-DTC), PEG-P (TMC-DTC)-Spe and PEG-P(TMC-DTC)-Cy5 at a mass ratio of 20/79/1 for cell entry and BBB transportation studies.

The size distribution, zeta potential, and stability of nano-formulations were determined using Zetasizer Nano-ZS and agarose gel electrophoresis, respectively. siRNA concentrations were measured by Nanodrop and quantified based on a calibration curve, and drug loading content (DLC) and efficiency (DLE) of siRNA were calculated according to the formula:

$$DLC\ (wt.\%) = (weight\ of\ loaded\ siSTAT3)/(total\ weight\ of\ polymer\ and\ siSTAT3) \times 100$$

$$DLE\ (\%) = (weight\ of\ loaded\ siSTAT3)/(weight\ of\ siSTAT3\ in\ feed) \times 100$$

The stability of Apstat3 was investigated during storage at 4 ℃ by tracking the changes in size and size distribution using DLS on days 0, 1, 3, 5, and 7. Changes in size and size distribution of Apstat3 in the presence 10% FBS at 48 h incubation were also monitored using DLS. Drug loading stability within polymersomes was studied using agarose gel electrophoresis. The following samples were applied: free siSTAT3, Pstat3, Apstat3, 10 mM GSH-pretreated Apstat3, 10 mM RNaseA-pretreated Apstat3. Briefly, 5 μL sample was mixed with 1 μL GelRed and loaded into the gels formed by 1 wt.% agarose and TAE. Electrophoresis was conducted at 80 V for 30 min, and the gels were photographed using gel imaging system.

2.5. Cellular uptake studies

GL261 cells in a 6-well plate (5×10^5/well) were cultured overnight to ca. 70% confluence, and fresh medium was replenished. Cy5-labeled Apstat3 and Pstat3 (cy5 conc.: 2 nM) were then added. After 4 h incubation, cells were digested with trypsin, centrifuged (1000 rpm, 3 min), washed twice with PBS, and resuspended in 300 μL PBS. FC analysis was performed within 1 h, and the data was analyzed using FlowJo_V10 software.

BMDCs freshly obtained were placed in a 6-well plate (1×10^6/well) and added with Cy5-labeled Apstat3 and Pstat3 (cy5 conc.: 2 nM) to incubate for 4 h. All cells including loosely adherent cells were collected, centrifuged (350 × g, 5 min), and treated as above before FC measurements.

2.6. In vitro cytotoxicity assays

GL261 cells in 96-well plates (5×10^3/well) were cultured overnight. 10 μL of formulations of free siSTAT3, Pstat3, or Apstat3 were added (siSTAT3 concentration: 0, 20, 50, 100 nM). After 48 h incubation, CCK-8 assays were performed and absorbance at 450 nm was measured using a microplate reader to calculate cell viability (n = 5). Toxicity of Apstat3 on bEnd3 (1×10^4/well) and BV2 (1×10^4/well) cells was investigated using the same protocol (n = 5). Toxicity of empty polymersomes, Aps and Ps, toward GL261 cells was evaluated with polymer concentrations of 0.1, 0.2, 0.5 and 1.0 mg/mL (n = 5). To study the effect of Apstat3 on the sensitization of GL261 cells and TMZ-resistant GL261 (GL261-R) cells to TMZ, TMZ was added to all wells except PBS group, followed by addition of PBS or Apstat3. After incubation for 48 h, CCK-8 assays were conducted, and half maximal inhibitory concentrations (IC_{50}) were calculated using Prism software (n = 5).

2.7. Cell apoptosis study

GL261 cells in 6-well plates (5×10^5/well) were cultured for 24 h, and

Apstat3, TMZ or TMZ+Apstat3 (siRNA: 50 nM; TMZ: 12.5 μg/mL) were added. After incubation for 12 h, culture medium was replaced with fresh medium, and cells were further cultured for 36 h. Cells were then collected, washed with PBS, and resuspended in 500 μL PBS for Annexin V-APC/7-AAD apoptosis assays and measured using flow cytometry (n = 3).

2.8. Evaluation of proliferation, migration and invasion of GL261 cells

To assess the effect of Apstat3 on the clone formation, GL261 cells seeded into 6-well plates (3000/well) were cultured for 24 h, and free siSTAT3, Pstat3, Apstat3, TMZ, or combo group TMZ+Apstat3 (siRNA: 20 nM, TMZ: 5 μg/mL) were added. After 12 h, culture medium was changed with fresh medium, and medium was refreshed every 2 days thereafter. After a total of 10 days of culturing, cells were fixed with 4% paraformaldehyde for 20 min, stained with 1% crystal violet for 30 min, washed, and then photographed (n = 3). Semi-quantitative analysis of grayscale was performed using ImageJ software.

To assess cell migration inhibition, GL261 cells in 6-well plates (1.5×10^5/well) were cultured for 12 h, and a scratch wound was created by gently scraping the cell layer with the tip of a 1-mL pipette. After washing, free siSTAT3, Pstat3, Apstat3, TMZ, or combo group TMZ+Apstat3 (siRNA: 20 nM, TMZ: 5 μg/mL) were added. After 12 h incubation, culture medium was replaced with fresh medium to incubate further for 24 h. Immediately after creating the scratch and after 24 h incubation, cells in the scratch area were imaged under a microscope, and the width of the scratches was semi-quantitatively using ImageJ software (n = 3).

To assess cell invasion inhibition, GL261 cells were pre-treated by incubation with free siSTAT3, Pstat3, Apstat3, TMZ, or combo group TMZ+Apstat3 (siRNA: 20 nM, TMZ: 5 μg/mL) for 12 h followed by medium exchange and further 36 h culture. A transwell model was built by plating 200 μL 2.5% matrigel on the insert, on which those pre-treated GL261 cells (1×10^5/mL, serum-free) was seeded in the upper chamber, with addition of 600 μL 20% FBS containing medium to the lower chamber. After the transwells were incubated for 48 h, the inserts were removed, cells that penetrated through the matrigel and insert membrane were stained with Calcein AM for 10 min and washed with PBS (3×). The inserts with cells were imaged and semi-quantitatively using ImageJ software (n = 3).

2.9. In vitro examination of the BBB penetration

A BBB model was built using a transwell with bEnd.3 cell monolayer in upper chamber and GL261 cells in the lower chamber. Briefly, bEnd.3 cells (2.0×10^5) were seeded on the insert (pore size: 1.0 μm) of the upper chamber (200 μL DMEM medium). At the TEER values of the monolayer above 200 $\Omega\cdot cm^2$ (maintained above 200 $\Omega\cdot cm^2$ throughout the experiment), GL261 cells were plated in the lower chamber for 12 h to adhere. Then Cy5-labeled Apstat3 or Pstat3 was added to the upper chambers (Cy5 concentration: 2 nM). At incubation times of 6, 12, and 24 h, GL261 cells were collected, and the mean fluorescence intensity (MFI) of Cy5 within GL261 cells was measured by flow cytometry.

2.10. Determination of mRNA and protein expression in GL261 cells

To study gene silencing effect, GL261 cells were cultured in 6-well plates (5×10^5/well) overnight, and incubated with free siSTAT3, Pstat3, Apstat3 (siRNA: 50 nM) or PBS (n = 3). After 12 h, culture medium was replaced with fresh medium and cells were further cultured for 36 h. Cells were harvested and total RNA was isolated and purified from cell lysate using RNA-easy Isolation Reagent. mRNA expression of STAT3 and MGMT was determined using qRT-PCR (glyceraldehyde-3-phosphate dehydrogenase (GAPDH) as internal reference) and analyzed using $2^{-\Delta\Delta CT}$ method.

To study the effect of Apstat3 on sensitization of GL261 cells to TMZ therapy, GL261 cells were treated with free siSTAT3, Pstat3, Apstat3, TMZ, or TMZ+Apstat3 (siRNA: 50 nM, TMZ: 12.5 μg/mL, n = 3) and the following procedures were the same as above to measure mRNA expressions of STAT3, MGMT, vascular endothelial growth factor (VEGF), phosphoinositide 3-kinase (PI3K), matrix metalloproteinase-9 (MMP9), and matrix metalloproteinase-2 (MMP2).

For WB analysis of protein expression, GL261 cells were treated the same as above and then lysed with RIPA. Proteins were isolated, purified and quantified before electrophoresis (20 μg) using standard procedure (PowerPac™, n = 3). Primary antibodies targeting STAT3, pSTAT3, MGMT, and Bcl-2, and HRP-labeled secondary antibody were used. Band images were taken using chemiluminescence detector and quantified using ImageJ software (GAPDH as internal reference).

2.11. Cultivation of TMZ-resistant GL261 cells (GL261-R)

GL261-R cells was conducted according to the reference [21] with modifications. GL261 cells (2.0×10^6/well) in cell culture dishes were sequentially incubated with TMZ at 1, 2, 5, 10, and 20 μg/mL. At each step cells were cultured for 2–3 passages until cells grew to the same density as GL261 cells without treatment. TMZ concentration of 20 μg/mL was selected for further culturing stable GL261-R. The cells needed to be regularly checked to ensure the maintenance of the drug resistance. GL261-R cells were then subjected to CCK-8 assays to assess the drug resistance, to WB experiments to evaluate the upregulation of STAT3 genes in these cells and the effect of transfection efficacy of Apstat3 in these GL261-R cells.

2.12. Maturation and transfection efficacy in BMDCs

To study the stimulation of DCs, BMDCs in a 12-well plate (1×10^6/well) were incubated with PBS, free siSTAT3, Pstat3, or Apstat3 (siRNA: 100 nM, n = 3). After 24 h, cells were collected, centrifuged (350 × g, 5 min), and washed twice with PBS. Cells were then labeled by with FITC-αCD11c, APC-αCD80, and PE-αCD86 antibodies at 4 °C in the dark for 30 min. Following another wash with PBS, cells were resuspended in 300 μL of PBS, and measured using flow cytometry to quantify $CD11c^+CD80^+CD86^+$ mDCs.

To study the downregulation of STAT3 gene and protein in BMDCs by siSTAT3 formulations, BMDCs in a 12-well plate (1×10^6/well) were incubated with PBS, free siSTAT3, Pstat3, or Apstat3 (siRNA: 100 nM, n = 3) for 48 h. The cells were then treated and measured as in section 2.10.

To investigate the STAT3 mRNA level within DCs in a tumor microenvironment (TME) mimicking condition, a transwell model was built by plating GL261 cells (5×10^5/mL) in the upper chamber and BMDCs (1×10^6/mL) in the lower chamber. TFG-β (10 ng/mL) was then added to both chambers to simulate TME conditions. After co-incubation for 12 h, the upper chambers were removed, and Apstat3, Pstat3 (siRNA: 100 nM) or PBS were added to the lower chambers to incubate for 48 h. DCs were taken and STAT3 mRNA expression was determined (n = 3).

2.13. Competitive endocytosis of Apstat3 by BMDCs and tumor cells

GL261 cells plated in 6-well plate (1×10^6 cells) were stained with CM-DIL (10 mM) for 2 h in the dark and cultured for 24 h to allow adherence. Then BMDCs (5×10^5 cells) were mixed, and Cy5-labeled Apstat3 and Pstat3 were added. After co-incubation for 4 h, cells were collected and stained with FITC-αCD11c antibody and PE/Cy7-αCD80 antibody by incubating at 4 °C for 30 min in the dark. Cells were subject to flow cytometry measurement (n = 3), and culture medium was taken for ELISA measurements of IL-6 and TNF-α concentrations (n = 3).

2.14. In vivo imaging and ex vivo imaging of mice

To evaluate the GBM-targeting property of Apstat3 in vivo, three

days after GL261 tumor implantation, mice were intravenously administered with 200 μL of Cy5-labeled Apstat3 or Pstat3 (0.5 μg cy5 per mouse). In vivo imaging of the mouse heads was performed at 4, 8, and 12 h post-injection. At 12 h, mice were euthanized, and the brains were harvested for ex vivo imaging.

To visualize the therapeutic efficacy of TMZ+Apstat3 treatment in mice bearing orthotopic GL261 tumors expressing luciferase (Luc), on days 3, 5, 7, 9, and 11 post tumor-implantation, the mice were injected with 200 μL of Apstat3 (4 mg/kg (mpk)) via tail veins and then TMZ (40 mpk) was given orally (n = 3). Mice received PBS were used as control group. On days 3, 7, 11, and 15, the tumor growth kinetics were assessed by intraperitoneal injection of D-luciferin potassium salt (75 mpk), followed by scanning of mouse heads using an in vivo imaging system. On day 15, mice were quickly intravenously administered 200 μL of Evans blue (0.5%). Mice were euthanized, and brain tissues were harvested and photographed using a smartphone camera.

2.15. Anti-tumor efficacy of Apstat3 in combination with TMZ in orthotopic GL261 model

All animal experiments were approved by the Animal Care and Use Committee of Soochow University (P. R. China) and all protocols for the animal studies conformed to the Guide for the Care and Use of Laboratory Animals (approval numbers: 202307A0300, 202503A0568).

Orthotopic GL261 tumor-bearing mouse models were established in female C57BL/6 mice from Charles River Company (6–8 weeks old, Beijing) by stereotactic injection of GL261 cells (1×10^5 cells in 5 μL cold PBS containing 50% Matrigel) into the left striatum (2.0 mm lateral, 0.5 mm posterior, 2.5 mm deep) [20]. The syringe was held still for 5 min post-injection. The day of injection was designated as day 0. Three days after GL261 tumor implantation, to preliminarily study the efficacy of the therapy (n = 3), on days 3, 5, 7, 9, and 11, the mice were injected with 200 μL of PBS or Apstat3 (4 mpk) via tail veins injection. TMZ (40 mpk) was administered orally for 5 consecutive days from day 3 to day 7. Body weights of the mice were monitored every 2 days, and the survival was recorded.

To evaluate the effect of Apstat3 doses in the combo group TMZ+Apstat3, on days 3, 5, 7, 9, and 11, the mice were i.v. injected with Apstat3 (1, 2 or 4 mpk) and then TMZ (40 mpk) was given orally as above (n = 5). To further investigate the boosting effect of anti-CTLA4 antibody on mouse survival, the mice were treated with Apstat3 (i.v., 4 mpk) and TMZ (p.o., 40 mpk) as above and i.v. injected with anti-CTLA4 (1 mpk) on days 7, 9, and 11 (n = 5). Body weight and survival of the mice were similarly recorded.

2.16. Statistical analysis

GraphPad Prism 8.0 was used for statistical analysis. Data was presented as mean ± standard deviation. Significant differences among groups were determined using one-way ANOVA with Tukey's multiple comparison tests. Kaplan-Meier survival rates were analyzed using the log-rank test for comparison. Statistical significance was defined as follows: * $p < 0.05$ means significant difference, ** $p < 0.01$, *** $p < 0.001$ and **** $p < 0.0001$ indicate highly significant difference.

3. Results and discussion

3.1. Preparation of ApoE peptide-functionalized siSTAT3-loaded polymersomes (Apstat3)

The formulation of Apstat3 was achieved by combining PEG-P(TMC-DTC)-Spe and ApoE-PEG-P(DTC-TMC) (mass ratio: 80/20) in a phosphate buffer containing siSTAT3, resulting in a highly reproducible preparation method (Fig. 1A). The siRNA loading efficiencies exceeded 90% at theoretical loading contents below 10 wt.%, with the resulting polymersomes exhibiting sizes ranging from 52 to 60 nm with narrow distributions and neutral zeta potential (Fig. 1B, Table S1). The high siRNA loading capability can be attributed to the electrostatic interactions between siSTAT3 and the spe component of the inner shell, in addition to the protective role of the crosslinked membrane against premature release [27]. For subsequent studies, Apstat3 loaded with 10 wt.% siSTAT3 was used unless otherwise stated. A non-targeting control, Pstat3, was prepared using only PEG-P(TMC-DTC)-Spe through the same methodology to facilitate comparative analyses. Size tracking results using DLS revealed the excellent colloidal stability of Apstat3, showing minimal variations in size and size distribution when stored at 4 °C over a period of 7 days, and when incubated in a 10% serum buffer for 48 h (Fig. 1C, D). Additionally, agarose gel electrophoresis confirmed the stability of Apstat3, revealing negligible leakage of siRNA and robust protection against enzymatic degradation. Importantly, the release of siRNA was triggered under cytosol-mimicking reductive conditions (pH 7.4, 10 mM GSH) (Fig. 1E–G). This specific release profile is particularly advantageous for subsequent in vitro and in vivo applications, as it facilitates controlled siRNA delivery in response to the intracellular environment, enhancing therapeutic efficacy against GBM.

3.2. Endocytosis, STAT3 silencing and BBB penetration of Apstat3

To investigate the endocytosis and intracellular release of Apstat3, Cy5-labeled Apstat3 was applied in GL261 cells. Flow cytometry analysis displayed that after 4-h incubation, the fluorescence intensity of Apstat3 group was 5.8-fold greater than Pstat3 group (Fig. 2A). This observation was further corroborated by CLSM results, suggesting that ApoE peptide effectively promotes endocytosis via receptor-ligand interactions. ApoE peptide was reportedly to target LDLRs, including LRP-1, LRP-2 and LDLR [28], which are overexpressed in GBM cells [19]. CLSM images also demonstrated a significant reduction in the co-localization of polymersome (Cy5) and endosomes (stained by Lysotracker), particularly in the Apstat3 group (Fig. 2B). This reduced co-localization indicates improved endosomal escape, an essential prerequisite for the silencing of the target STAT3 gene in cytoplasm.

The effects of Apstat3 on STAT3 and MGMT expressions in GL261 cells were then studied. The qRT-PCR results demonstrated that free siSTAT3 had no effect compared to PBS control, while Pstat3 significantly reduced STAT3 mRNA levels (*) and Apstat3 further enhanced this silencing effect (*) (Fig. 2C). WB analyses corroborated these findings, revealing that Apstat3 markedly decreased STAT3 expression compared to free siSTAT3 and Pstat3 groups (Fig. 2D). Moreover, treatment with Apstat3 resulted in a downregulation of MGMT at both mRNA and protein levels (Fig. 2C, D). This downregulation may be attributed to the well-documented interactions in which STAT3 activation promotes MGMT upregulation [29]. Given that MGMT is a principal drive for acquired resistance to TMZ [30], the reduced expression of MGMT via Apstat3 treatment validates its potential for enhancing combination therapy with TMZ.

The CCK-8 assay results demonstrated that Apstat3 induced a significant cytotoxicity in GL261 cells at siSTAT3 concentration of 50 and 100 nM, contrasting with the non-toxicity observed with free siSTAT3 and Pstat3 (**, Fig. 2E). This cytotoxic effect is likely due to the targeted downregulation of STAT3 pathway, which is crucial for tumor proliferation and invasion [31]. Importantly, Apstat3 exhibited no adverse effects on bEnd.3 and BV2 at the same concentrations (Fig. 2F), and empty vehicles showed no toxicity (Fig. 2G). These results confirm that the cytostatic effect of siSTAT3 delivered by Apstat3 selectively induces apoptosis in GL261 cells.

To evaluate the BBB penetration capabilities of Apstat3, we employed a bEnd.3 monolayer model in a transwell system. Apstat3 was added to upper chamber, with GL261 cells seeded in lower chamber. Flow cytometry analysis revealed that the uptake of Apstat3 in GL261 cells illustrated ca. 1.6, 3.8, and 4.0-fold increases after 6, 12, and 24 h, respectively, compared to Pstat3 group (Fig. 2H). This enhanced BBB penetration of Apstat3 is attributed to the targeting ability of ApoE

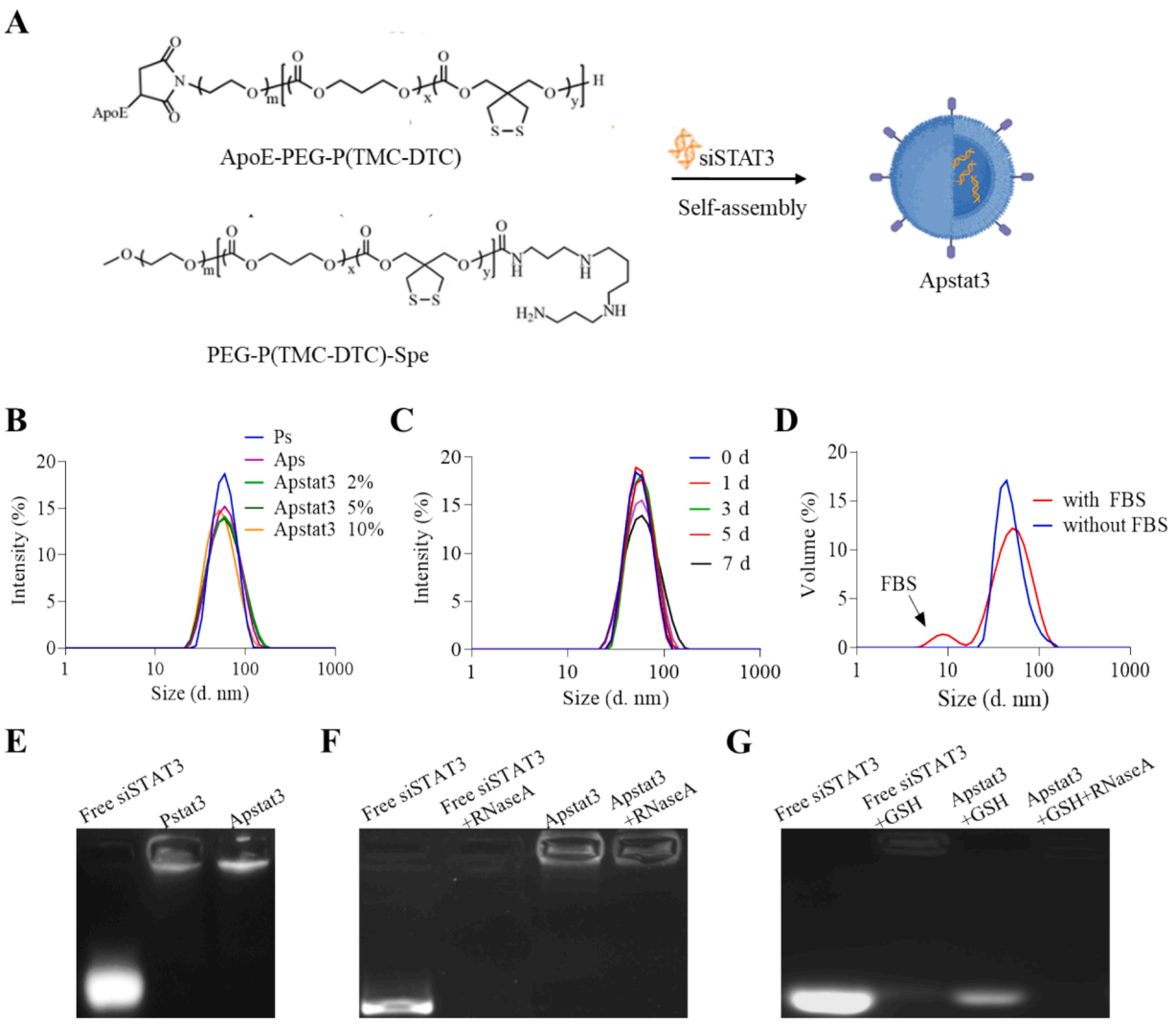

Fig. 1. Characterization of Apstat3. (A) Preparation of Apstat3. (B) Size and size distribution of empty polymersomes Ps and Aps, and Apstat3 loaded with 2%, 5%, and 10% siSTAT3, as measured by DLS. Changes in size distributions of Apstat3 (C) after 7-day storage at 4 °C or (D) in 10% serum-containing phosphate buffer for 48 h. Gel electrophoresis analysis of (E) siSTAT3 loading and leakage of Apstat3 (drug loading of 10 wt.%), and (F) protection of siSTAT3 by polymersomes after treatment with ribonuclease A (10 mM, 1 h) and (G) triggered release by GSH (10 mM, 6 h).

peptide to LDLRs present on both the BBB and GL261 cells, holding promise for improving the therapeutic efficacy of GBM treatments.

3.3. Apstat3 sensitized GL261 cells to TMZ therapy by downregulating STAT3 and MGMT

The abnormal activation of the STAT3 pathway in GBM is known to contribute to resistance against TMZ therapy [32]. The ability of Apstat3 to effective knockdown STAT3 and MGMT positions it as a promising candidate for enhancing the efficacy of TMZ, particularly in the context of drug resistance driven by MGMT upregulation. To assess the synergistic potential of TMZ and Apstat3, CCK-8 assays were conducted, illustrating that the combination therapy (TMZ+Apstat3) induced the most potent cytotoxicity with the lowest IC_{50} (49.8 μg/mL), and a combination index (CI, 0.46) in GL261 cells, indicative of a strong synergistic effect (Fig. 3A). The order of administration of TMZ and Apstat3 appeared to have no influence on the cell viability (Fig. 3B), suggesting that both agents can be combined flexibly in therapeutic applications. Furthermore, TMZ+Apstat3 treatment caused a marked increase in apoptotic cell populations (32.1%), significantly higher than Apstat3 (17.1%) and TMZ (10.2%) monotherapies (**, Fig. 3C), further highlighting the synergistic nature of this therapeutic combination.

Subsequently, we explored the effects of TMZ+Apstat3 therapy on the expression of genes associated with TMZ resistance and apoptosis, specifically STAT3, MGMT, and Bcl-2 in GL261 cells. qRT-PCR results revealed that TMZ+Apstat3 treatment notably inhibited the expression of all three genes, demonstrating a significantly stronger effect than either TMZ alone, which showed no effect, or the Apstat3 monotherapy, which elicited moderate downregulation (*, Fig. 3D). WB confirmed that TMZ + Apstat3 therapy elicited superior knockdown of STAT3, pSTAT3, MGMT and Bcl-2 (Fig. 3E). Particularly, the silencing effects of Bcl-2 and MGMT were very significant compared to monotherapies. The inhibition of STAT3 pathway consequently blocked the activation of Bcl-2 and VEGF, while also leading to reduced MGMT expression, corroborating findings from Kang et al. [33]. The results validate that the TMZ+Apstat3 therapy possesses the ability to enhance the efficacy of TMZ and promote tumor cell apoptosis, effectively mitigating TMZ resistance.

Given that drug resistance often occurs in GBM patients receiving TMZ therapy, we then investigated the efficacy of our therapy in GL261-R cells. The resistant cells often show increased MGMT expression that in turn accelerate the degree of drug resistance [34]. These GL261-R cells exhibited heightened expressions of MGMT, STAT3, pSTAT3 and Bcl-2 compared to the parental GL261 cells, as demonstrated by WB analysis (Fig. 3F). Notably, TMZ monotherapy exhibited 2.6-fold increased

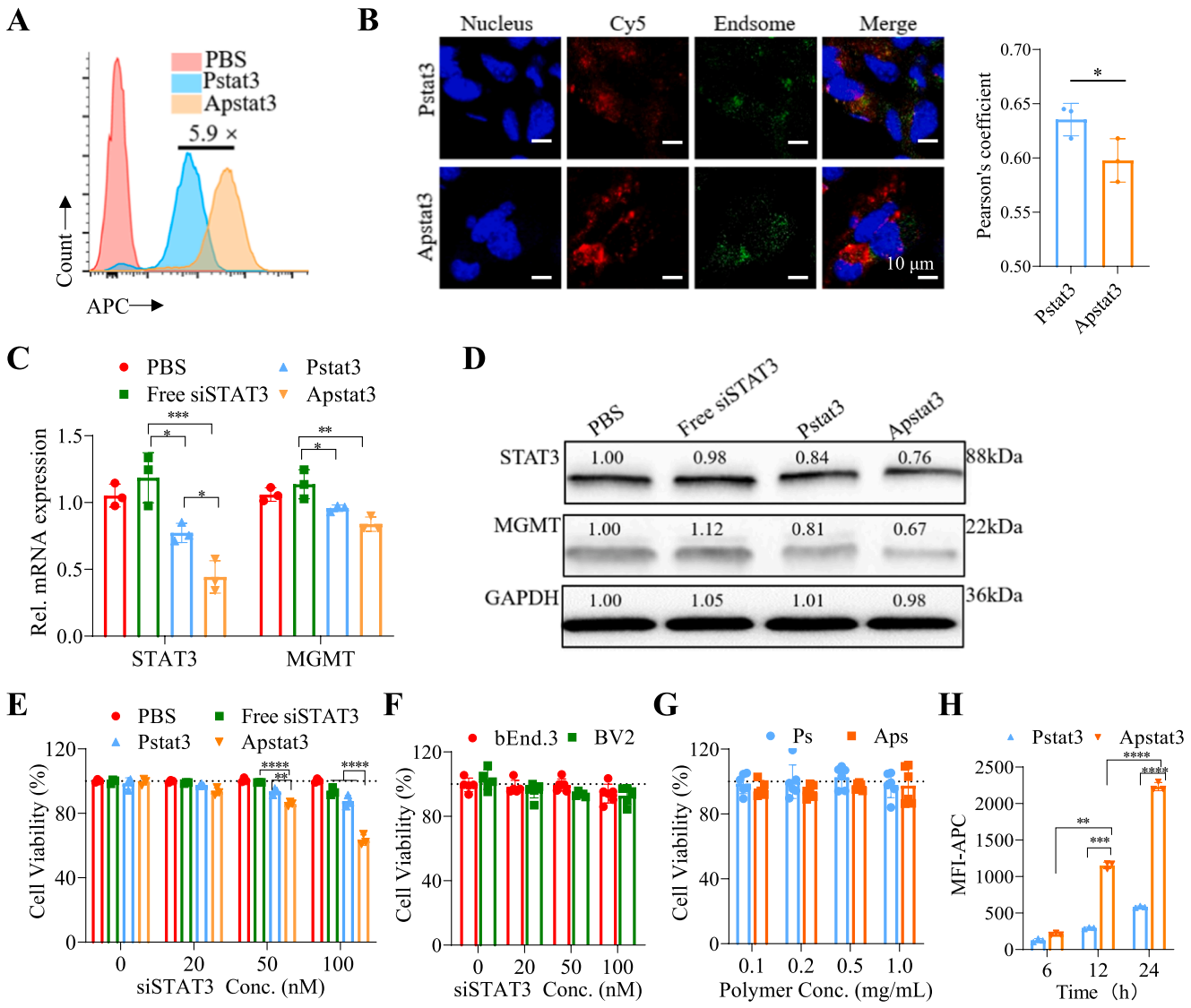

Fig. 2. Endocytosis, gene silencing, cytotoxicity and BBB transportation of Apstat3 in vitro. (A) Endocytosis and (B) endosomal escape of Cy5-labeled Apstat3 at 4 h incubation with GL261 cells with Pearson coefficient of Cy5 and lysotracker green analyzed using ImageJ (scale bar: 10 μm). Expressions of (C) mRNA (n = 3) and (D) protein of STAT3 and MGMT in GL261 cells after 12 h treatment with Apstat3, Pstat3 or free siStat3 (GAPGH as internal reference). Cytotoxicity of Apstat3 toward (E) GL261 cells, (F) bEnd.3 and BV2 cells, as well as (G) cytotoxicity of empty polymersomes, Ps and Aps, toward GL261 cells at 48 h incubation (n = 5). (H) Mean fluorescence intensity (MFI) of Cy5-labeled Apstat3 and Pstat3 within GL261 cells in the lower chamber of a transwell model (Apstat3 initially added into the upper chamber) at 6, 12 and 24 h (n = 3). (For interpretation of the references to colour in this figure legend, the reader is referred to the web version of this article.)

IC_{50} in GL261-R cells relative to the normal GL261 cells (Fig. 3G), confirming the development of TMZ resistance. Remarkably, the TMZ+Apstat3 treatment could not only greatly inhibit the expression of pSTAT3, Bcl-2 and MGMT in GL261-R cells (Fig. 3F), but also significantly reduced the IC_{50} by threefold (Fig. 3H). These findings illustrate the potential of TMZ+Apstat3 therapy in overcoming TMZ resistance in GBM treatment.

3.4. Inhibition of proliferation, migration and invasion by TMZ+Apstat3 in GL261 cells

To further explore the therapeutic potential of the TMZ+Apstat3 combination, we evaluated its effects on the proliferation, migration and invasion of GL261 cells. The upregulation of STAT3 and MGMT has been implicated in the growth and invasion behavior of GBM cells, contributing to their resistance to conventional therapies [35]. Clone formation assays demonstrated that neither free siSTAT3 nor Pstat3 greatly influenced the proliferative capacity of GL261 cells. In contrast, both Apstat3 and TMZ monotherapies could significantly inhibit clone formation (****), likely attributable to their ability to induce tumor cell death and decrease the expression of stemness and proliferation-related genes. Remarkably, TMZ+Apstat3 treatment further significantly suppressed the clone formation (**, Fig. 4A).

Wound-healing assays were conducted to assess cell migration. Observations showed rapid migration of cells in the PBS group, with complete scratch closure within 48 h. Treatments with free siSTAT3, Pstat3, Apstat3 or TMZ inhibited cell migration to varying degrees; however, TMZ+Apstat3 therapy significantly suppressed the cell migration preventing scratch healing (****, Fig. 4B). Given the invasive nature of GBM, characterized by its capacity to infiltrate the surrounding stroma and normal tissues, we employed a transwell invasion model utilizing a stroma-mimicking gel-coated insert to assess the invasion capability of GL261 cells under the influence of TMZ+Apstat3. Live/dead staining results revealed that the number of viable cells traversing the stroma was moderately reduced in the free siSTAT3, Pstat3, Apstat3 or TMZ groups compared to PBS control. Remarkably, the TMZ+Apstat3

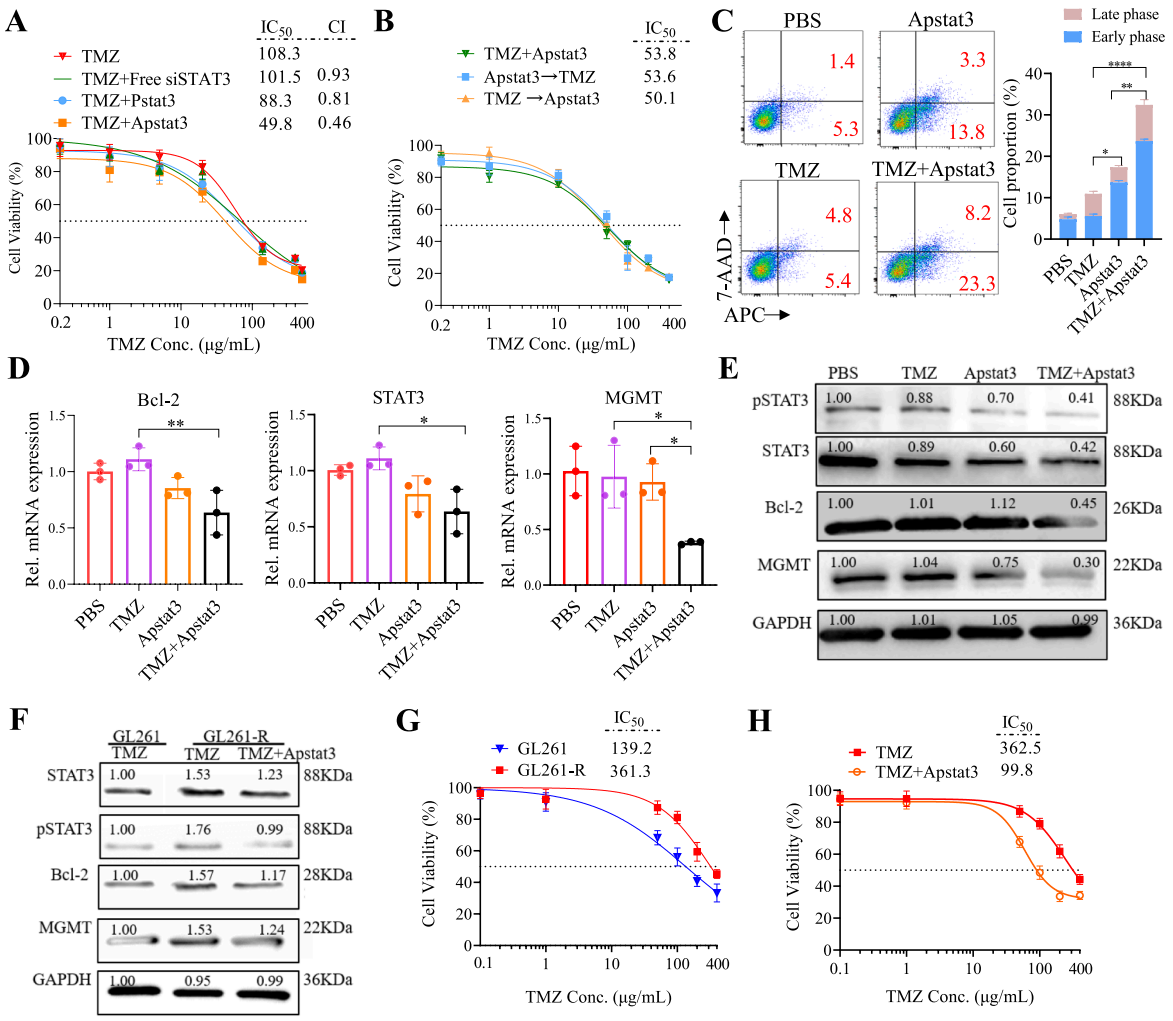

Fig. 3. Sensitization of GL261 cells by Apstat3 to TMZ treatment. Viability of GL261 cells treated with (A) TMZ alone and its combination with Apstat3, or (B) TMZ+Apstat3 combination therapy with various treatment orders (n = 5). (C) Apoptosis analysis of GL261 cells induced by TMZ+Apstat3 at 48 h incubation (n = 3). Expression levels of (D) mRNA (n = 3) and (E) protein of STAT3, pSTAT3, Bcl-2 and MGMT in tumor cells as analyzed by qRT-PCR and WB, respectively. (F) Expression of STAT3, pSTAT3, Bcl-2 and MGMT in TMZ-resistant GL261-R cells after treatment with Apstat3. (G) Viability of GL261 cells and GL261-R cells treated with free TMZ for 48 h (n = 5). (H) Viability of GL261-R cells at 48 h incubation with TMZ and TMZ+Apstat3 (n = 5).

group exhibited the least number of cells invading through the stroma, echoing its superior inhibitory efficacy in cell invasion (Fig. 4C).

We further investigated the expression levels of genes associated with proliferation, migration, and invasion, specifically VEGF, PI3K/AKT, MMP9, and MMP2, through qRT-PCR experiments. Among three siSTAT3 formulations, Apstat3 exhibited the highest capacity for downregulating these genes. TMZ alone had low or no influence on them. In contrast, TMZ+Apstat3 therapy resulted in a further reduction in the expression of four genes, particularly for MMP2 and MMP9 (Fig. 4D). Cell proliferation is intricately regulated by specific signaling pathways and proteins like VEGF, PI3K/AKT [36]. MMP2 is particularly involved in tumor-related angiogenesis by releasing pro-angiogenic factors, and MMP9 promotes tumor invasion and metastasis by decomposing the extracellular matrixes [37]. The observed down-regulation of these pathways and genes by TMZ+Apstat3 treatment underscores its superior inhibitory effect on the proliferation, migration, and invasion of GBM cells, which are critical determinants of patient prognosis.

3.5. Modulation of immune responses by Apstat3 in BMDCs

Apstat3 may serve as a potent stimulator of immune responses, particularly by influencing DCs and regulatory T cells (Tregs), given the crucial role of STAT3 in these immune cell types [38]. Aberrant activation of STAT3 in DCs has been reported to suppress their anti-tumor capability by inhibiting maturation and antigen presentation [39]. To investigate the effects of Apstat3 on BMDCs, we analyzed their uptake and maturation after exposure to Apstat3. Flow cytometry results showed that Apstat3 and Pstat3 exhibited little difference in the entry into BMDCs (Fig. 5A), and similarly enhanced stimulation capacity with a proportion of mature DCs (mDCs, $CD11c^+CD80^+CD86^+$) of ca. 33.3%, which was significantly higher than PBS and free siSTAT3 groups (*, Fig. 5B). The great activation of BMDCs is likely attributed to the downregulation of STAT3, as confirmed by WB analyses that demonstrated effective STAT3 silencing. While Apstat3 illustrated superior silencing capacity compared to Pstat3 (Fig. 5C), owing to its enhanced endosomal escape ability in DCs.

Within TME, STAT3 is often constitutively activated in DCs, leading to reduced expression of major histocompatibility complex II and costimulatory molecules, thereby impairing antigen-presenting functions and contributing to the overall immunosuppression characteristic of GBM [13,40]. In light of this, inhibiting STAT3 in DCs not only promotes their maturation but also enhances the effector functions of DCs and T cells, collectively aiding in halting tumor progression. To study the effect of Apstat3 on the STAT3 expression of DCs under TME-mimicking conditions, we established a transwell co-culture model involving

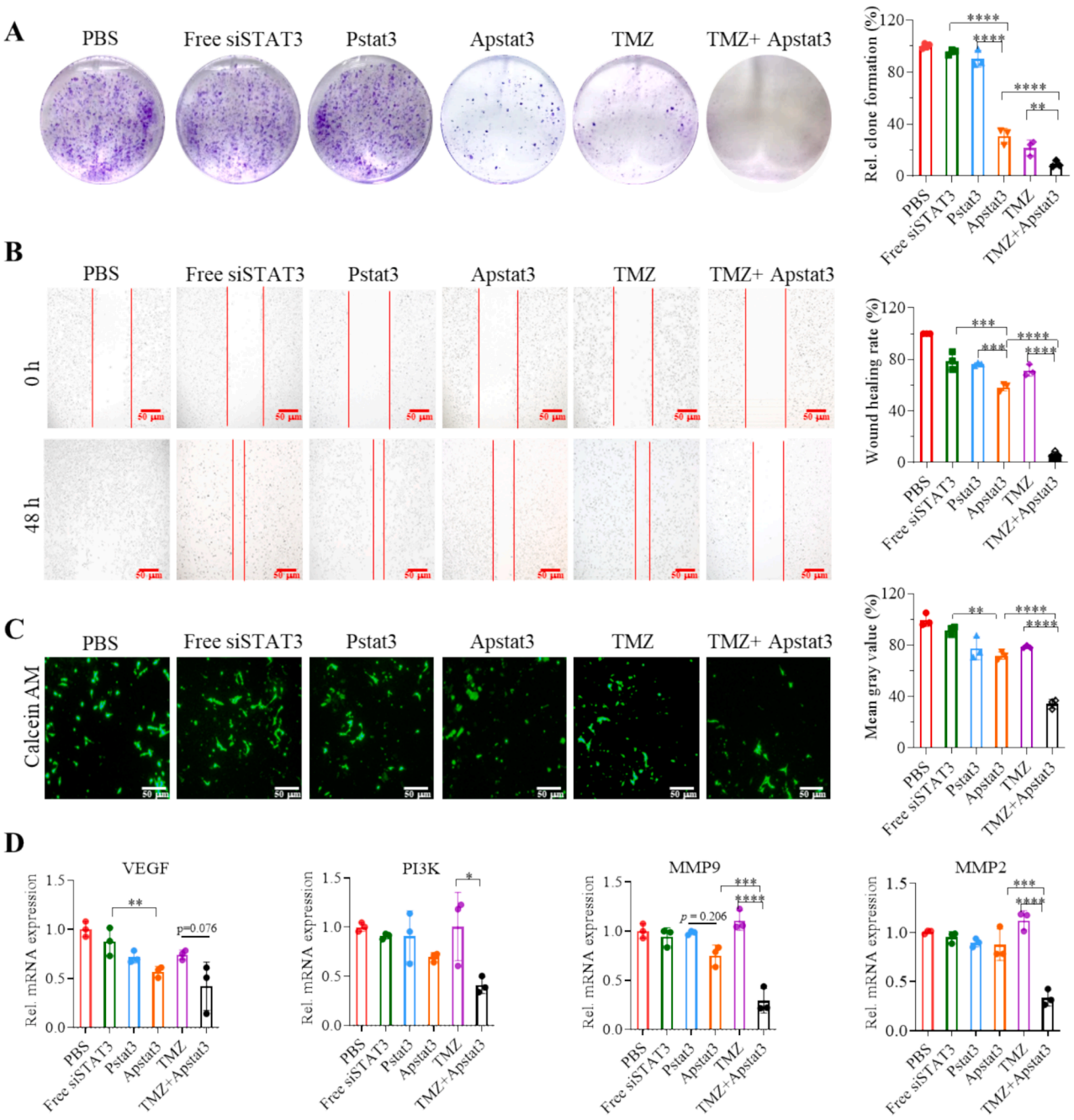

Fig. 4. Effects of Apstat3 and TMZ+Apstat3 on the proliferation, migration and invasion of GL261 cells (n = 3). (A) Images and analyses of the formation clones at 10-day incubation. (B) Images and analysis of wound healing at 48 h incubation (scale bar: 50 μm). (C) Images and analyses of live cells transported through the gels of the insert in a transwell model at 24 h incubation (scale bar: 50 μm). (D) Expression of VEGF, PI3K, MMP9 and MMP2 mRNA in GL261 cells at 12 h incubation.

GL261 cells and BMDCs stimulated with TGF-β (Fig. 5D). Co-cultured BMDCs induced significantly increased STAT3 mRNA levels compared to cells without stimulation of GL261 cells (**), underscoring the importance of STAT3 down regulation in TME. Remarkably, the treatment with Apstat3 substantially downregulated STAT3 mRNA (**, Fig. 5D).

Tumor cells and their microenvironment can affect the immune responses, converting some immune cells into suppressive cells (such as Tregs) and thereby weakening the immune response [41]. To further study the competitive uptake of Apstat3 in a model that simulates the TME, we co-incubated BMDCs with CM-DIL-stained GL261 cells for 4 h, followed by adding Cy5-labeled Apstat3 or Pstat3. After 4 h, $Cy5^+$ percentages in both GL261 cells and BMDCs as well as DC activation were measured using flow cytometry (Fig. 5E). The analysis showed high $Cy5^+$ proportions in both DC and tumor cell populations in quadrants Q1, Q2, and Q4 (Q1 represents BMDCs that took up GL261 cells), indicating efficient endocytosis of the nanoformulations by both cell types (Fig. 5F). Importantly, Apstat3 demonstrated notably higher endocytosis efficiency compared to Pstat3 (*, Fig. 5G).

Moreover, the proportions of mature DCs (mDCs, $CD11c^+CD80^+$) in Apstat3-treated group was significantly greater than Pstat3 group (**, Fig. 5H), suggesting that the direct effects of Apstat3, in conjunction with its indirect effects on tumor cells, collectively contributed to the activation of DCs. Furthermore, the Apstat3 treatment secreted ca. 6-fold proinflammatory cytokines, including IL-6 and TNF-α (Fig. 5I). Such cytokines not only exert cytotoxic effects on tumor cells but may

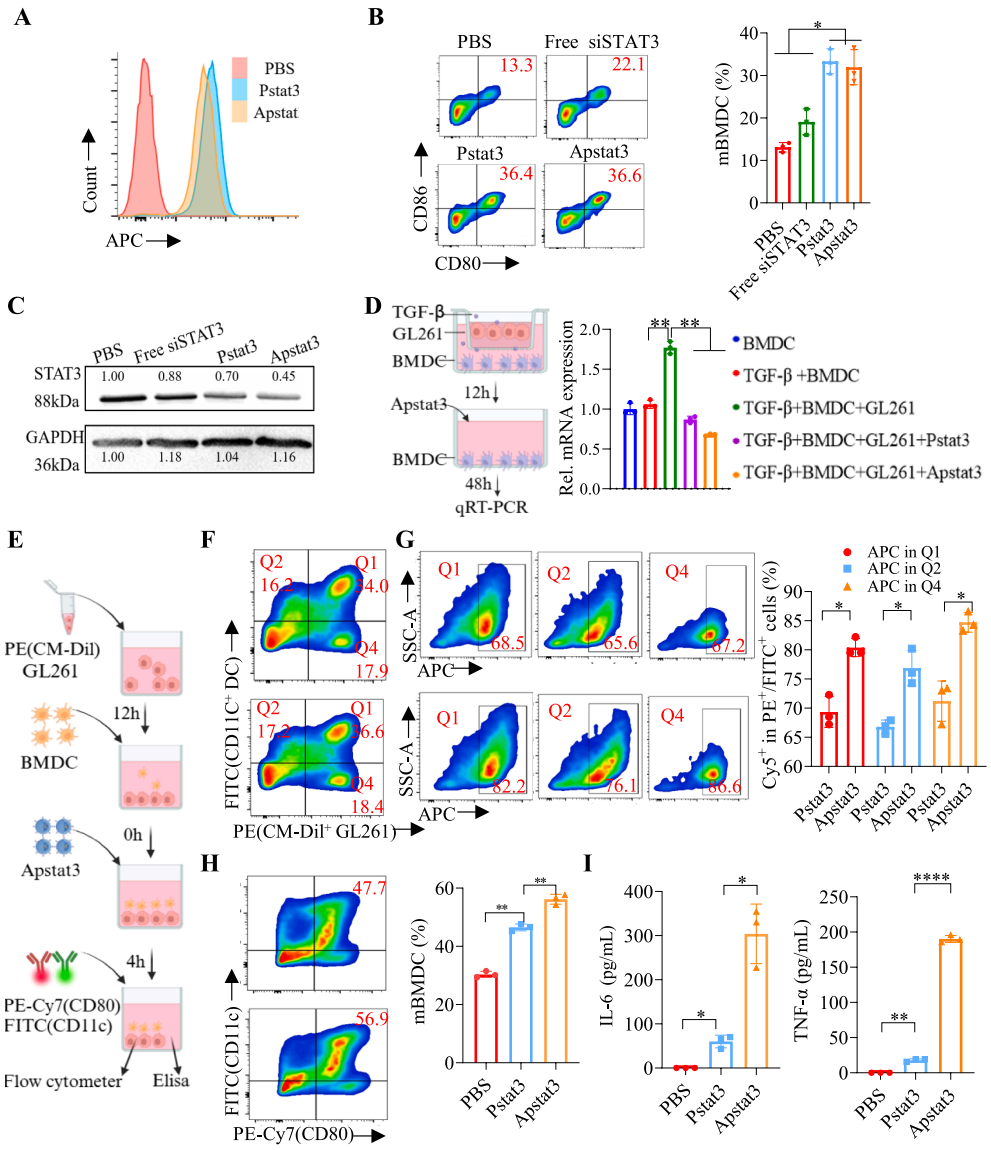

Fig. 5. Effects of Apstat3 on the activation, gene silencing and competitive uptake of BMDCs. (A) Endocytosis of Apstat3 by BMDCs at 4 h incubation. (B) Proportions of mature DCs (mDCs, $CD80^{+}CD86^{+}$) at 24 h incubation with Apstat3 (n = 3). (C) Downregulation of STAT3 in BMDCs at 48 h incubation. (D) Expression of STAT3 mRNA within DCs in a TME mimicking condition (co-cultured with GL261 tumor cells and TFG-β) at 12 h incubation (n = 3). (E) Schematic experimental flow of competitive uptake of Cy5-labled Apstat3 by GL261 cells and BMDCs at 4 h co-incubation (for Fig. 5F-5I). (F) $Cy5^{+}$ percentages in GL261 cells and BMDCs (n = 3), (G) $Cy5^{+}$ percentages in Q1, Q2 and Q4 regions, and (H) proportions of mDCs as measured by flow cytometry, as well as (I) concentrations of secreted IL-6 and TNF-α (n = 3).

also serve as chemokines to recruit additional immune cells to TME, halting tumor progression [42]. These results confirm that the aberrantly activated STAT3 in DCs within TME can be downregulated by Apstat3, thus reshaping the immunosuppressive TME, besides direct effect on the tumor cells.

3.6. *Anti-GBM activity of TMZ+Apstat3 in orthotopic GL261 tumor model*

The in vivo anti-GBM effects of TMZ+Apstat3 therapy were preliminarily studied in an orthotopic GL261 mouse model established through stereotactic injection of GL261 cells in the brains of C57BL/6 mice [43]. This orthotopic model better recapitulates the human glioma microenvironment by maintaining the BBB structure as compared to subcutaneous models, enabling more clinically relevant assessment of drug efficacy and disease progression. GL261 cell line, derived from C57BL/6 mice, exhibits high host compatibility and reliable tumorigenicity, particularly suitable for evaluating tumor-immune interactions and therapeutic efficacy in immunotherapy. Firstly, in vivo imaging of orthotopic GL261 models revealed that Apstat3 accumulated significantly higher in GBM tumors compared to Pstat3 (Fig. S1A, B), confirming the ability of Apstat3 to effectively cross the BBB and target brain tumors. In a subsequent preliminary study, at three days of post-inoculation, mice were administered a regimen of five oral doses of TMZ 40 mpk and five intravenous injections of Apstat3 at 4 mpk (Fig. S2A). TMZ was administered at a human-equivalent dose, converted from clinical dose in patients. Monitoring body weight changes of these mice is critical, as significant weight loss often precedes severe health deterioration and mortality within 48 h [20]. Here, body weights of PBS and Apstat3 groups declined by day 16, yielding a median survival time (MST) of 18 days. TMZ alone notably postponed the onset of weight loss, extending the MST by 7 days (*). In contrast, TMZ+Apstat3 therapy significantly prolonged the MST to 34 days with one out of three mice tumor-free, validating the in vivo synergistic effect of Apstat3 and

TMZ treatment.

Subsequent investigations evaluated the efficacy of TMZ combined with varying doses of siSTAT3 (1, 2 and 4 mpk), while maintaining at fixed TMZ dose of 40 mpk (Fig. 6A). The results showed that as Apstat3 dose increased, the drop in body weight was progressively delayed (Fig. 6B), with the MST significantly extending from 31 days for TMZ group to 34, 38, and 44 days for the increasing Apstat3 doses, respectively (Fig. 6C). Our results suggest that for highly malignant GBM, the administration of high doses of drugs, below toxicity thresholds in early stage, is crucial for rapidly targeting tumor cells, alleviating resistance, and ultimately prolonging survival. Additionally, an in vivo bioluminescence imaging study revealed significantly suppressed signals in the brains of TMZ+Apstat3 group compared to PBS group by day 15 (Fig. S3). This was further highlighted with over 10-fold lower signals in the ex vivo imaging and nearly no blue coloration of tumor-bearing brains (Fig. 6D, E). While the brains of PBS group showed clear Evans blue extravasation due to compromised BBB integrity.

Nevertheless, TMZ+Apstat3 therapy did not achieve complete remission. The curative approach for GBM is often hindered by the immunosuppressive TME and inherent heterogeneity of GBM [44,45]. Tregs are important immunosuppressive cells in the GBM TME [46], as they downregulate the secretion of pro-inflammatory cytokines such as interleukin 2 and interferon-γ, thereby inhibiting the function of APCs. To study the effect of Apstat3 on Tregs, we extracted the spleen from a GL261 mouse, and splenic T cells were treated with Apstat3 for 48 h (Fig. S4A). Flow cytometry results showed a tenfold increase in Treg populations in GL261 mouse compared to healthy mouse (****), confirming the presence of an immunosuppressive environment in GBM. Remarkably, Apstat3 treatment significantly reduced the proportion of Tregs (*, Fig. S4B), validating its capability to diminish tumor immune evasion and promote anti-tumor immune responses.

To enhance anti-GBM efficacy and survival benefits, we subsequently

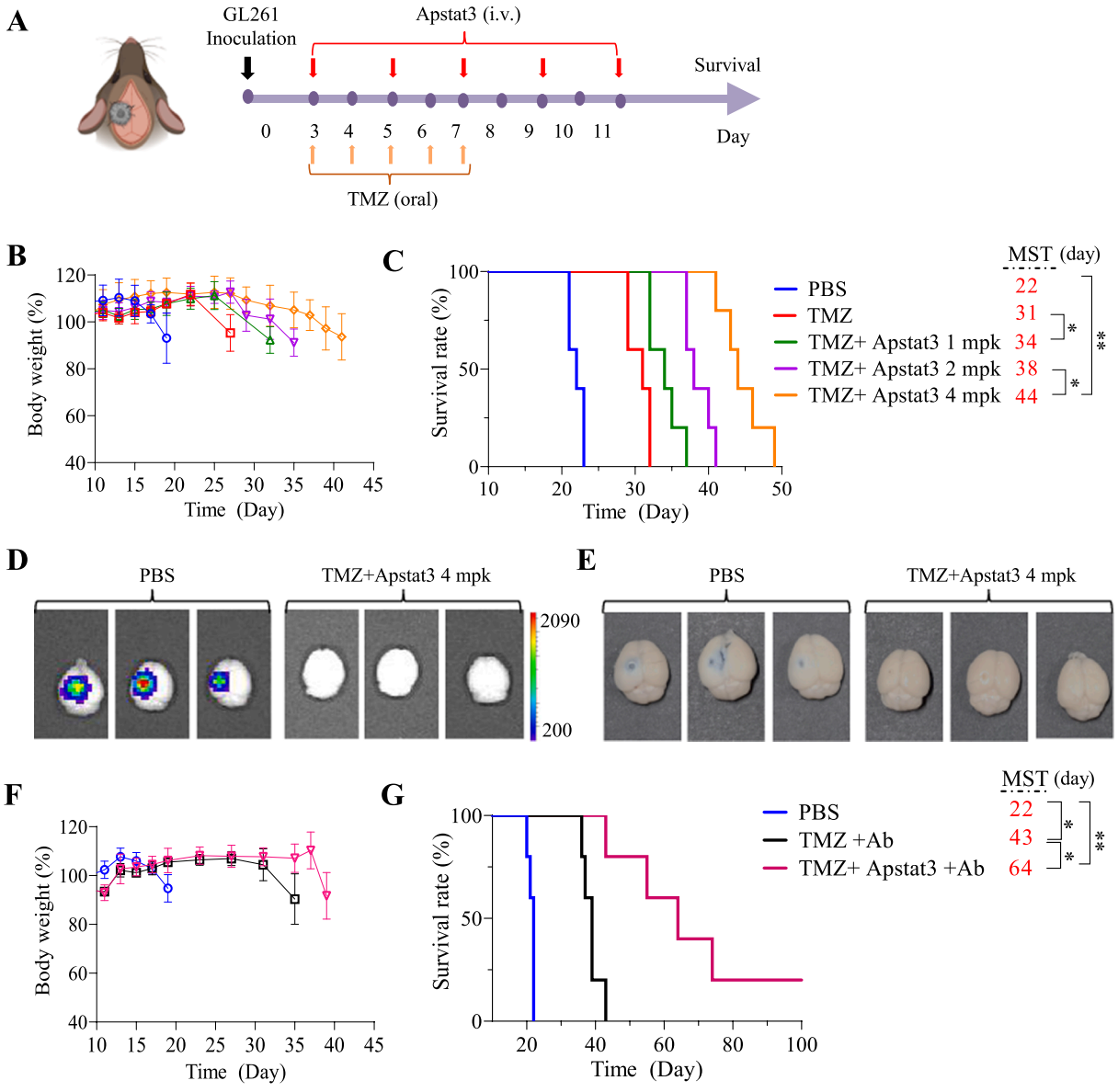

Fig. 6. Therapeutic efficacy of Apstat3 and in its combination therapies in orthotopic GL261 tumor-bearing mice. (A) Experimental schedule. (B) Body weight changes and (C) survival rates of the mice treated with TMZ+Apstat3 with various siSTAT3 dosages (siRNA: 1, 2, 4 mpk, TMZ: 40 mpk, n = 5). (D) The ex vivo brain bioluminescence images and (E) cerebral Evans blue extravasation at day 15 after treatment with TMZ+Apstat3 (siRNA: 4 mpk, TMZ: 40 mpk, n = 3). (F) Body weight changes and (G) survival rates of the mice treated with TMZ+Apstat3+Ab (siRNA: 4 mpk, TMZ: 40 mpk, Ab: 1 mpk, n = 5). (For interpretation of the references to colour in this figure legend, the reader is referred to the web version of this article.)

combined ICB therapy, anti-CTLA4 antibody (Ab), with TMZ+Apstat3 therapy. Remarkably, this triple therapy of TMZ+Apstat3+Ab significantly extended the lifespan of the mice, yielding MST of 64 days (*), with 20% of the mice achieving complete remission (Fig. 6G). This contrasts to TMZ+Ab and TMZ groups with MST of 43 and 31 days, respectively (Fig. 6F, G). These compelling results suggest that in the context of immunosuppressive GBM, the incorporation of anti-CTLA4 antibody can effectively modulate the TME, facilitating enhanced sensitivity to chemotherapy.

4. Conclusion

In this study, we demonstrate that ApoE peptide-modified polymersomes encapsulating siSTAT3 (Apstat3) as a novel brain-targeted nanotherapeutic platform that effectively combat GBM when combined with TMZ chemotherapy and anti-CTLA4 immunotherapy. Our approach addresses critical challenges in GBM therapy by achieving efficient BBB penetration and tumor-specific delivery, leading to effective silencing of STAT3 and MGMT—key drivers of GBM progression and drug resistance. Apstat3 exhibits optimal small size, stable encapsulation, and efficient cellular uptake by both GBM cells and tumor-infiltrating DCs, which results in suppression of tumor proliferation, invasion and immunosuppressive signaling, while promoting DC maturation and proinflammatory cytokine secretion. Compared to previous treatments hindered by poor BBB penetration, TMZ resistance, and suboptimal targeting of tumor and immune components [47,48], our work innovatively combines brain-targeted polymersome nanocarriers with RNAi technology to overcome these obstacles. In orthotopic GL261 mouse models, systemic injection of Apstat3 with oral TMZ greatly prolongs survival, and the combination of anti-CTLA4 checkpoint blockade further improves therapeutic outcomes, achieving complete remission in 20% of the treated mice. Importantly, the polymersome platform utilizes biocompatible, biodegradable components including polyethylene glycol, polycarbonate and spermine, which support favorable safety and manufacturing profiles conducive to clinical translation. Going forward, this study highlights the potential of the nanodelivery of siRNA to simultaneously target oncogenic and immunosuppressive pathways in GBM. Future work will focus on optimization of dosing regimens and further exploration of combinatorial immunotherapies to maximize therapeutic benefit. Overall, Apstat3 represents a significant advancement in the field of nanomedicine-based glioma therapy, offering a versatile and effective strategy to surmount the formidable challenges posed by GBM's aggressiveness and therapeutic resistance.

CRediT authorship contribution statement

Mingyu Xia: Writing – original draft, Investigation, Formal analysis, Data curation. **Songsong Zhao:** Validation, Methodology, Formal analysis, Data curation. **Zhiwei Sun:** Investigation, Formal analysis. **Yan Shi:** Investigation, Formal analysis. **Wenhai Lin:** Resources, Methodology. **Zhiyuan Zhong:** Writing – review & editing, Supervision, Resources, Conceptualization. **Fenghua Meng:** Writing – review & editing, Validation, Supervision, Project administration, Funding acquisition, Conceptualization.

Declaration of competing interest

The authors declare that they have no known competing financial interests or personal relationships that could have appeared to influence the work reported in this paper.

Acknowledgement

This work is supported by research grants from the National Natural Science Foundation of China (NSFC 52473142, 52033006). The authors thank Biorender.com for the assistance in illustrations.

Appendix A. Supplementary data

Supplementary data to this article can be found online at https://doi.org/10.1016/j.jcis.2025.137751.

Data availability

Data will be made available on request.

References

[1] S.M. Robbins, D.L. Senger, Targeting network circuitry in glioma, Nature Cancer 4 (10) (2023) 1406–1407.
[2] H. Zarabi, R. Wicks, G. Russel, D. Banderage, R. Strowd, R. Mott, A. Laxton, S. Tatter, J. White, H.W. Lo, W. Debinski, M. Chan, G. Lesser, C. Cramer, Clinical outcomes for high risk who grade II glioma patients treated with upfront tmz-based chemoradiotherapy, Neurooncology 24 (2022) 52.
[3] M. Abate, M. Porru, V. Campani, C. Leonetti, V. Nele, R. Di Paola, M. De Martino, M. Russo, M. Tathode, A.M. Cossu, M. Bocchetti, A. Angelillo, M. Ianniello, N. Petrillo, G. Savarese, R. Della Monica, L. Chiariotti, R. Addeo, M. Caraglia, G. De Rosa, S. Zappavigna, Self-assembling nanoparticles for delivery of miR-603 and miR-221 in glioblastoma as a new strategy to overcome resistance to temozolomide, J. Control. Release 377 (2025) 458–469.
[4] M.S. Tomar, A. Kumar, C. Srivastava, A. Shrivastava, Elucidating the mechanisms of temozolomide resistance in gliomas and the strategies to overcome the resistance, Bba-Rev Cancer 1876 (2) (2021) 188616.
[5] L. De Roeck, C.R. Gillebert, R.C.M. van Aert, A. Vanmeenen, M. Klein, M.J. B. Taphoorn, K. Gehring, M. Lambrecht, C. Sleurs, Cognitive outcomes after multimodal treatment in adult glioma patients: A meta-analysis, Neurooncology 25 (8) (2023) 1395–1414.
[6] J.X. Yin, X.F. Wang, X. Ge, F.S. Ding, Z.M. Shi, Z.H. Ge, G. Huang, N.W. Zhao, D. Y. Chen, J.X. Zhang, S. Agnihotri, Y.D. Cao, J. Ji, F. Lin, Q.H. Wang, Q.G. Zhou, X. X. Wang, Y.P. You, Z.M. Lu, X. Qian, Hypoxanthine phosphoribosyl transferase 1 metabolizes temozolomide to activate AMPK for driving chemoresistance of glioblastomas, Nat. Commun. 14 (1) (2023) 5913.
[7] L. Rong, N. Li, Z.Z. Zhang, Emerging therapies for glioblastoma: current state and future directions, J. Exp. Clin. Canc. Res. 41 (1) (2022) 142.
[8] N.A. Mohile, H. Messersmith, N.T. Gatson, A.F. Hottinger, A. Lassman, J. Morton, D. Ney, P.L. Nghiemphu, A. Olar, J. Olson, J. Perry, J. Portnow, D. Schiff, A. Shannon, H.A. Shih, R. Strowd, M. van den Bent, M. Ziu, J. Blakeley, Therapy for Diffuse Astrocytic and Oligodendroglial Tumors in Adults: ASCO-SNO Guideline, J. Clin. Oncol. 40 (4) (2022) 403-+.
[9] J. Biau, E. Thivat, E. Chautard, D. Stefan, M. Boone, B. Chauffert, C. Bourgne, D. Richard, I. Molnar, S. Levesque, R. Bellini, F. Kwiatkowski, L. Karayan-Tapon, P. Verrelle, C. Godfraind, X. Durando, Phase 1 trial of ralimetinib (LY2228820) with radiotherapy plus concomitant temozolomide in the treatment of newly diagnosed glioblastoma, Radiother. Oncol. 154 (2021) 227–234.
[10] F. Khan, Y.Y. Lin, H. Ali, L.Z. Pang, M. Dunterman, W.H. Hsu, K. Frenis, R.G. Rowe, D.A. Wainwright, K. McCortney, L.K. Billingham, J. Miska, C. Horbinski, M. S. Lesniak, P.W. Chen, Lactate dehydrogenase a regulates tumor-macrophage symbiosis to promote glioblastoma progression, Nat. Commun. 15 (1) (2024) 1987.
[11] T.M. Ayele, Z.T. Muche, A.B. Teklemariam, A.B. Kassie, E.C. Abebe, Role of JAK2/STAT3 signaling pathway in the tumorigenesis, chemotherapy resistance, and treatment of solid tumors: a systemic review, J. Inflamm. Res. 15 (2022) 1349–1364.
[12] W.H. Huang, Z. Zhong, C. Luo, Y.Z. Xiao, L.M. Li, X. Zhang, L. Yang, K. Xiao, Y. C. Ning, L. Chen, Q. Liu, X. Hu, J. Zhang, X.F. Ding, S.L. Xiang, The miR-26a/AP-2α/Nanog signaling axis mediates stem cell self-renewal and temozolomide resistance in glioma, Theranostics 9 (19) (2019) 5497–5516.
[13] S.L. Zou, Q.Y. Tong, B.W. Liu, W. Huang, Y. Tian, X.H. Fu, Targeting STAT3 in cancer immunotherapy, Mol. Cancer 19 (1) (2020) 145.
[14] P.S. Thilakasiri, R.S. Dmello, T.L. Nero, M.W. Parker, M. Ernst, A.L. Chand, Repurposing of drugs as STAT3 inhibitors for cancer therapy, Semin. Cancer Biol. 68 (2021) 31–46.
[15] M. Sanati, C.G. Figueroa-Espada, E.L. Han, M.J. Mitchell, S.A. Yavari, Bioengineered nanomaterials for siRNA therapy of chemoresistant cancers, ACS Nano 18 (51) (2024) 34425–34463.
[16] F. Araste, A. Aliabadi, K. Abnous, S.M. Taghdisi, M. Ramezani, M. Alibolandi, Self-assembled polymeric vesicles: Focus on polymersomes in cancer treatment, J. Control. Release 330 (2021) 502–528.
[17] R. Huang, H. Du, L. Cheng, P.Z. Zhang, F.H. Meng, Z.Y. Zhong, Targeted nanodelivery of siRNA against *KRAS G12D* inhibits pancreatic cancer, Acta Biomater. 168 (2023) 529–539.
[18] B.Q. Song, M.R. Wu, L.J. Qin, W.J. Liang, X. Wang, Smart Design of Targeted Drug Delivery System for Precise Drug Delivery and Visual Treatment of Brain Gliomas, Adv. Healthc. Mater. 14 (4) (2025) 2402967.
[19] J. Zhang, B. Liu, C.W. Xu, C.C. Ji, A.A. Yin, Y.F. Liu, Y. Yao, B.W. Li, T.D. Chen, L. L. Shen, Y.M. Wu, Cholesterol homeostasis confers glioma malignancy triggered by hnRNPA2B1-dependent regulation of SREBP2 and LDLR, Neurooncology 26 (4) (2024) 684–700.

[20] J.J. Wei, D. Wu, Y. Shao, B.B. Guo, J.J. Jiang, J. Chen, J.P. Zhang, F.H. Meng, Z. Y. Zhong, ApoE-mediated systemic nanodelivery of granzyme B and CpG for enhanced glioma immunotherapy, J. Control. Release 347 (2022) 68–77.
[21] W.Y. He, X.Z. Li, M. Morsch, M. Ismail, Y.J. Liu, F.U. Rehman, D.Y. Zhang, Y. B. Wang, M. Zheng, R. Chung, Y. Zou, B.Y. Shi, Brain-targeted codelivery of Bcl-2/Bcl-xl and Mcl-1 inhibitors by biomimetic nanoparticles for orthotopic glioblastoma therapy, ACS Nano 16 (4) (2022) 6293–6308.
[22] R. Moreira, C. Nobrega, L.P. de Almeida, L. Mendonca, Brain-targeted drug delivery - nanovesicles directed to specific brain cells by brain-targeting ligands, J. Nanobiotechnol. 22 (1) (2024) 260.
[23] M. Zheng, Q.L. Du, X. Wang, Y. Zhou, J. Li, X. Xia, Y.Q. Lu, J.L. Yin, Y. Zou, J. B. Park, B.Y. Shi, Tuning the Elasticity of Polymersomes for Brain Tumor Targeting, Adv. Sci. 8 (20) (2021) 2102001.
[24] P. Zhang, T.Z. Wang, G.H. Cui, R.N. Ye, W.J. Wan, T.H. Liu, Y.R. Zheng, Z. Y. Zhong, Systemic Multifunctional Nanovaccines for Potent Personalized Immunotherapy of Acute Myeloid Leukemia, Adv. Mater. 36 (40) (2024) 2407189.
[25] J.J. Wei, D. Wu, S.S. Zhao, Y. Shao, Y.F. Xia, D.W. Ni, X.Y. Qiu, J.P. Zhang, J. Chen, F.H. Meng, Z.Y. Zhong, Immunotherapy of Malignant Glioma by Noninvasive Administration of TLR9 Agonist CpG Nano-Immunoadjuvant, Adv. Sci. 9 (13) (2022) 2103689.
[26] B.B. Guo, Y. Qu, Y.P. Sun, S.S. Zhao, J.D. Yuan, P.Z. Zhang, Z.Y. Zhong, F.H. Meng, Co-delivery of gemcitabine and paclitaxel plus nanoCpG empowers chemoimmunotherapy of postoperative "cold" triple-negative breast cancer, Bioact. Mater. 25 (2023) 61–72.
[27] F. Adams, C.M. Zimmermann, D. Baldassi, T.M. Pehl, P. Weingarten, I. Kachel, M. Kraenzlein, D.C. Jürgens, P. Braubach, I. Alexopoulos, M. Wygrecka, O. M. Merkel, Pulmonary siRNA delivery with sophisticated amphiphilic poly (spermine acrylamides) for the treatment of lung fibrosis, Small 20 (22) (2024) 2308775.
[28] J.L. Guo, D. Braun, G.A. Fitzgerald, Y.-T. Hsieh, L. Rouge, A. Litvinchuk, M. Steffek, N.E. Propson, C.M. Heffner, C. Discenza, S.J. Han, A. Rana, L.L. Skuja, B.Q. Lin, E. W. Sun, S.S. Davis, S. Balasundar, I. Becerra, J.C. Dugas, C. Ha, J. Hsiao-Nakamoto, F. Huang, S. Jain, J.E. Kung, N.P.D. Liau, C.S. Mahon, H.N. Nguyen, N. Nguyen, M. Samaddar, Y. Shi, D. Tatarakis, Y. Tian, Y. Zhu, J.H. Suh, T. Sandmann, M.E. K. Calvert, A. Arguello, L.A. Kane, J.W. Lewcock, D.M. Holtzman, C.M. Koth, G. Di Paolo, Decreased lipidated ApoE-receptor interactions confer protection against pathogenicity of ApoE and its lipid cargoes in lysosomes, Cell 188 (2024) 1–20.
[29] S. Kumari, R. Gupta, R.K. Ambasta, P. Kumar, Multiple therapeutic approaches of glioblastoma multiforme: From terminal to therapy, Bba-Rev. Cancer 1878 (4) (2023) 188913.
[30] B. Oldrini, N. Vaquero-Siguero, Q.H. Mu, P. Kroon, Y. Zhang, M. Galán-Ganga, Z. S. Bao, Z. Wang, H.J. Liu, J.K. Sa, J.F. Zhao, H. Kim, S. Rodriguez-Perales, D. H. Nam, R.G.W. Verhaak, R. Rabadan, T. Jiang, J.G. Wang, M. Squatrito, MGMT genomic rearrangements contribute to chemotherapy resistance in gliomas, Nat. Commun. 11 (1) (2020) 3883.
[31] J. Yin, Y. Seo, J. Rhim, X. Jin, T.H. Kim, S.S. Kim, J.H. Hong, H.S. Gwak, H. Yoo, J. B. Park, J.H. Kim, Cross-talk between PARN and EGFR-STAT3 signaling facilitates self-renewal and proliferation of glioblastoma stem cells, Cancer Res. 83 (22) (2023) 3693–3709.
[32] T. Jiang, Y.H. Qiao, W.M. Ruan, D.Y. Zhang, Q.S. Yang, G.Y. Wang, Q.Z. Chen, F. P. Zhu, J.L. Yin, Y. Zou, R.J. Qian, M. Zheng, B.Y. Shi, Cation-Free siRNA micelles as effective drug delivery platform and potent RNAi nanomedicines for glioblastoma therapy, Adv. Mater. 33 (45) (2021) 2104779.
[33] D.W. Kang, W.C. Hwang, Y.N. Noh, K.S. Park, D.S. Min, PhospholipaseD1inhibition sensitizes glioblastoma to temozolomide and suppresses its tumorigenicity, J. Pathol. 252 (3) (2020) 304–316.
[34] Z.Z. He, B. Peng, Q. Wang, J. Tian, P. Liu, J. Feng, Y.W. Liao, L.Y. Chen, P. Jia, J. Tang, Transcriptomic analysis identifies the neuropeptide cortistatin (CORT) as an inhibitor of temozolomide (TMZ) resistance by suppressing the NF-KB-MGMT signaling axis in human glioma, Genes Dis 11 (3) (2024) 100977.
[35] D.D. Shi, J.J. Tao, S.L. Man, N. Zhang, L. Ma, L.P. Guo, L.Q. Huang, W.Y. Gao, Structure, function, signaling pathways and clinical therapeutics: The translational potential of STAT3 as a target for cancer therapy, Bba-Rev. Cancer 1879 (6) (2024) 189207.
[36] K.T. Chan, S. Blake, H.R. Zhu, J. Kang, A.S. Trigos, P.B. Madhamshettiwar, J. Diesch, L. Paavolainen, P. Horvath, R.D. Hannan, A.J. George, E. Sanij, K. M. Hannan, K.J. Simpson, R.B. Pearson, A functional genetic screen defines the AKT-induced senescence signaling network, Cell Death Differ. 27 (2) (2020) 725–741.
[37] R.R. Fan, C.L. Chen, M. Mu, D. Chuan, H. Liu, H. Hou, J.H. Huang, A.P. Tong, G. Guo, J.G. Xu, Engineering MMP-2 activated nanoparticles carrying B7-H3 bispecific antibodies for ferroptosis-enhanced glioblastoma Immunotherapy, ACS Nano 17 (10) (2023) 9126–9139.
[38] Y.J. Li, C.Y. Zhang, A. Martincuks, A. Herrmann, H. Yu, STAT proteins in cancer: orchestration of metabolism, Nat. Rev. Cancer 23 (3) (2023) 115–134.
[39] H. Kitamura, Y. Ohno, Y. Toyoshima, J. Ohtake, S. Homma, H. Kawamura, N. Takahashi, A. Taketomi, Interleukin-6/STAT3 signaling as a promising target to improve the efficacy of cancer immunotherapy, Cancer Sci. 108 (10) (2017) 1947–1952.
[40] J.J. Wang, J.Y. Wang, W.X. Hong, L.L. Zhang, L.Q. Song, Q. Shi, Y.F. Shao, G. F. Hao, C.Y. Fang, Y.P. Qiu, L.J. Yang, Z.X. Yang, J.C. Wang, J. Cao, B. Yang, Q. J. He, Q.J. Weng, Optineurin modulates the maturation of dendritic cells to regulate autoimmunity through JAK2-STAT3 signaling, Nat. Commun. 12 (1) (2021) 6198.
[41] L.Y. Zhang, K. Kuca, L. You, Y.Y. Zhao, K. Musilek, E. Nepovimova, Q.H. Wu, W. D. Wu, V. Adam, Signal transducer and activator of transcription 3 signaling in tumor immune evasion, Pharmacology Therapeutics 230 (2022) 107969.
[42] A. Goenka, F. Khan, B. Verma, P. Sinha, C.C. Dmello, M.P. Jogalekar, P. Gangadaran, B.C. Ahn, Tumor microenvironment signaling and therapeutics in cancer progression, Cancer Commun. 43 (5) (2023) 525–561.
[43] G. Catania, G. Rodella, K. Vanvarenberg, V. Préat, A. Malfanti, Combination of hyaluronic acid conjugates with immunogenic cell death inducer and CpG for glioblastoma local chemo-immunotherapy elicits an immune response and induces long-term survival, Biomaterials 294 (2023) 122006.
[44] H. Lin, C.X. Liu, A.K. Hu, D.W. Zhang, H. Yang, Y. Mao, Understanding the immunosuppressive microenvironment of glioma: mechanistic insights and clinical perspectives, J. Hematol. Oncol. 17 (1) (2024) 31.
[45] A. Lauko, A.L.C. Lo, M.S. Ahluwalia, J.D. Lathia, Cancer cell heterogeneity & plasticity in glioblastoma and brain tumors, Semin. Cancer Biol. 82 (2022) 162–175.
[46] Z. Amoozgar, J. Kloepper, J. Ren, R.E. Tay, S.W. Kazer, E. Kiner, S. Krishnan, J. M. Posada, M. Ghosh, E. Mamessier, C. Wong, G.B. Ferraro, A. Batista, N. Wang, M. Badeaux, S. Roberge, L. Xu, P. Huang, A.K. Shalek, D. Fukumura, H.J. Kim, R. K. Jain, Targeting Treg cells with GITR activation alleviates resistance to immunotherapy in murine glioblastomas, Nat. Commun. 12 (1) (2021) 2582.
[47] B. Kasenda, D. König, M. Manni, R. Ritschard, U. Duthaler, E. Bartoszek, A. Bärenwaldt, S. Deuster, G. Hutter, D. Cordier, L. Mariani, J. Hench, S. Frank, S. Krähenbühl, A. Zippelius, C. Rochlitz, C. Mamot, A. Wicki, H. Läubli, Targeting immunoliposomes to EGFR-positive glioblastoma, ESMO Open 7 (1) (2022) 100365.
[48] M. Jezierzanski, N. Nafalska, M. Stopyra, T. Furgol, M. Miciak, J. Kabut, I. Gisterek-Grocholska, Temozolomide (TMZ) in the Treatment of Glioblastoma Multiforme-A Literature Review and Clinical Outcomes, Curr. Oncol. 31 (7) (2024) 3994–4002.